An extendable half-bridge dimmable multi-channel LED driver for DC/DC grid lighting applications

Behnam Abbasi Soltani[1], **Mehran Sabahi**[1, 2, *], **Ebrahim Babaei**[1, 2], **and Jaber Pouladi**[1]

[1] *Department of Electrical Engineering, Shabestar Branch, Islamic Azad University, Shabestar, Iran*
[2] *Faculty of Electrical and Computer Engineering, University of Tabriz, Tabriz, Iran*
[*] *Corresponding author: sabahi@tabrizu.ac.ir*

Manuscript received 14 February, 2021; revised 24 June, 2021; accepted 09 September, 2021. Paper no. JEMT-2102-1281.

In this paper, a light emitting diode (LED) driver with multiple outputs, suitable to use with DC grid supply, is proposed. The proposed LED driver provides the ability to individually control the brightness of each output channel. In order to control the output power of each channel, a burst control mode is employed resulting in reduction of conduction losses. Moreover, the half bridge switches are turned on and off at zero voltage (ZV) with a fixed switching frequency; therefore, the switching losses is reduced and efficiency is further increased. Design and implementation have been simplified by choosing the same structure of the resonant series for outputs. A two-channel DC/DC converter is simulated and experimentally tested to verify the theoretical analyses.

keywords: *Keywords: DC/DC Converter, driver, light-emitting-diode, multi-channel.*

http://dx.doi.org/10.22109/jemt.2021.273304.1281

1. INTRODUCTION

Nowadays, Lighting consumes a huge percentage of the world's energy. So improving the quality of LED drivers is an important issue. Some of the applications of LEDs are general architectural lighting, traffic lights, displays, street lighting, car lighting, greenhouse lighting, decorative lights, and display backlighting. LEDs have high lightening efficiency, compared to conventional lamps, and they consume low energy and have long lifespan (about 100,000 hours), also they do not have environmental contamination (no harmful elements such as mercury), have good colour rendering properties and high colour rending index (CRI), high reliability, low maintenance costs, compact size flexibility, and easy control [1–3].
Conventionally, the LED drivers are composed of AC-DC converters and DC-DC converters [4, 5]. Typically, the AC-DC converter is in charge of power factor corrections (PFC) and the DC/DC converter regulates the current of LED string to avoid LED flickering [6]. DC/DC converters play a very important role in power electronics converters [7–9]. Conventionally, multiple single-channel converters were used for multi-channel drivers [10, 11], which increased the circuit volume and price but today, a converter with multiple outputs is designed instead of multiple single-channel drivers. This type of design reduces the size of the control circuit and simplicity of control in intelligent lighting systems. Different multi-output AC-DC LED driver topologies are presented to apply in LED lamps; however, a few LED driver topologies are specially developed for DC grids could be found in literature.
Some other multi-channel DC/DC converters introduced in [10–13] that are not able to independently adjust the channel light and only have the ability to share the current between several channels equally. There are some converters that can adjust the channel light independently, but have a hard switching and as a result will have high losses and low efficiency [14–16]. Another multi-channel LED driver employing transformer and series switches with the LED strings is introduced in [10]. Using transformers need extra control circuits and increase complexity of structure and in addition electromagnetic devices have much losses and decrease efficiency. These converters suffer from many components and complexity. This driver also operates under hard switching and is bulky. A multichannel driver suitable for DC grid is proposed in [11]. This converter develops the half-bridge inverter by variable inductor (VI), transformer, and rectifier which is accompanied by soft switching operation. The use of variable inductors in each channel provides independent control of the light of each channel, but will be accompanied by an increase in the number of control elements and the complexity of the circuit. As the output power increases, the efficiency of these converters will decrease, especially in the case of multiple LED channels. In addition, in this method, the failure of an LED string in a channel seems to cause the imbalance of circuit, and the circuit efficiency decreases.
Normally in the conventional circuits, for each LED branch, a dimming switch is placed in series with the LED which operates

under hard switching and could lead to shock signals, damage to the LED bulb, and reduction in LED and the dimming switch lifespan. Furthermore, these methods have large pulsating problems of input/output and the electromagnetic interference (EMI) problem.

A multi-channel LED driver with half-bridge series resonant structure is presented in [12]. Current in different channels is balanced with main switches operating at below resonant frequencies. Switching below resonant frequency would result in discontinuous current mode (DCM) condition, which limits high power applications especially in multichannel drivers and further increases the harmonics of the output current. Moreover, the dimming capability is possible by replacing the resonant circuit components which means that online dimming is not done and requires new designing. As this driver operates in switching frequencies below resonant frequency, there is an increase in components size and the weight.

In this paper, a single-input multi-output (SIMO) half-bridge series resonant based LED driver with multiple outputs suitable for DC grid is proposed. The presented converter operates above resonant frequency to decrease total harmonic distortion and reduce the size and weight of the components. Therefore, it is suitable for high power application of multi-channel drivers. The dimming switch is employed in the series with SRC and it is controlled by burst control mode. In burst control mode, dimming switch is drive by number of pulses. In burst control mode method, switching frequency of main switches is fixed and EMI problems is eliminated [13]. In the Sections 2 and 3, the proposed converter is analysed and in Section 4, design sample is presented. In Section 5, simulation results are discussed to verify theoretically analysis and finally conclusion is presented in Section 6.

2. ANALYSIS OF THE PROPOSED LED DRIVER

Fig.1 shows the schematics of the proposed dimmable multi-channel LED driver suitable for DC grid applications. The proposed driver is composed of a half bridge and a separate circuit for each LED channel which include a SRC, a dimming switch, and an H-bridge rectifier. The multi-channel structure is presented by the modular structure for each LED channel, simplifying the design and manufacturing of the driver.

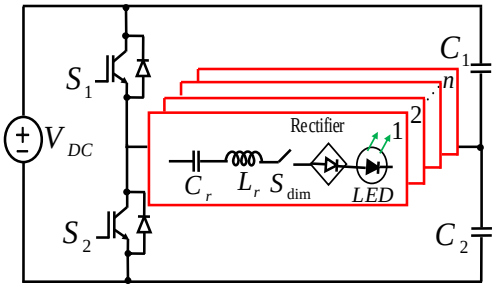

Fig. 1. Proposed dimmable multi-channel LED driver.

For analysing and better comprehension of the proposed driver, a detailed structure with one channel is illustrated in Fig.2. For ease of calculation, input voltage is assumed to be $2V_d$. S_1 and S_1 is switched at 50% duty cycle and provides symmetrical pulses with V_d amplitude. Dimming switch is called S_{dim} that controls the current of each LED channel.

Burst control mode is used for controlling of dimming switches. This strategy S_{dim} gate driving signal is shown in Fig.3. In order to regulate the brightness of each LED channel, an appropriate duty cycle is chosen to drive the dimming switch. The burst duty cycle D_{burst} is presented as $D_{burst} = T_{on}/T_{burst}$ where $T_{burst} = 1/f_{dim}$.

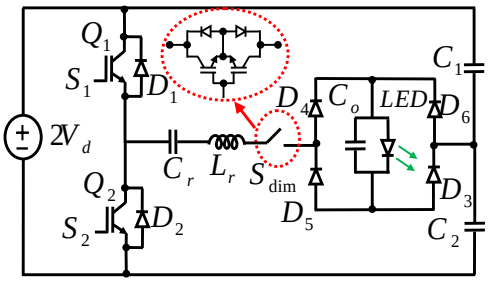

Fig. 2. The structure of the proposed driver with one channel.

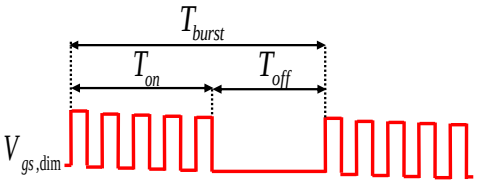

Fig. 3. Burst mode control of dimming switch.

In this manuscript T_{burst} is constant for all outputs and $D_{burst(j)}$ is set according to the required brightness of each output. Whenever the dimming switch is on, there are four different operational modes for the proposed driver; each mode is explained as follows and the relative topologies under different operational modes are shown in Fig. 4.

Mode 1 Fig. 4(a): During this mode, Q_1, D_4, and D_3 are conducting. This mode is finished when the switch S_1 is turned off.

Mode 2 Fig. 4(b): This interval begins by turning off switch S_2. As S_2 turns off, diode D_1 starts to conduct in order to resume the current of L_r. During this interval, switch S_1 could be turned on under ZVZCS. In this mode diodes D_1, D_5, and D_6 are on. This interval terminates whenever the current i_{Lr} reaches zero.

Mode 3 Fig. 4(c): As switch turns off, the antiparallel diode turns on. During this mode the switch could be turned on under ZVZCS. In this interval, D_2, D_3 and D_4 are on. Whenever the current decreases to zero, this mode ends.

Mode 4 Fig. 4(d): As soon as current i_{Lr} reaches zero, the direction of current i_{Lr} is reversed and Q_2 starts to conduct. In this mode, Q_2, D_5, and D_6 are on. At the end of this interval switch S_2 turns off.

For better comprehension of the driver's operation, the current of inductor L_r, voltage and current of switch S_1 during different operation modes are illustrated in Fig. 5. Equivalent and simplified circuits of the proposed driver in the different operational modes are shown in Fig. 6.

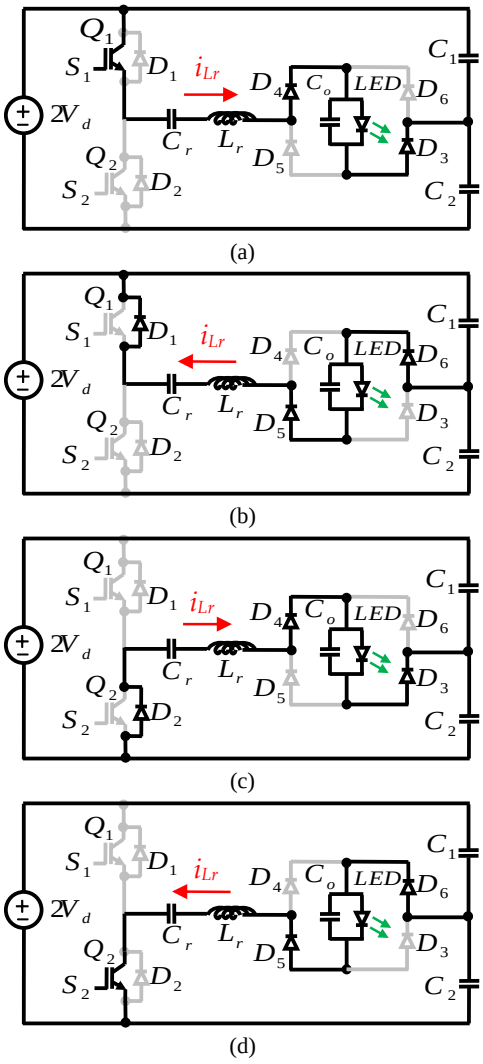

Fig. 4. The proposed driver's topology in (a) mode 1 (b) mode 2 (c) mode 3 (d) mode 4.

As indicated in the Fig. 6, equivalent circuits of the driver in different operational modes is an RLC circuit in series with different corresponding DC voltages. This DC voltage in different intervals is shown in Fig. 7.

Fourier series of Fig. 7 is figured out as follows:

$$v(t) = \frac{a_0}{2} + \sum_{n=1,3,5,\ldots}^{\infty} C_n \sin(n\omega t + \phi_n) \;\; ; \;\; C_n = \sqrt{{a_n}^2 + {b_n}^2} \tag{1}$$

where a_n, and b_n are Fourier coefficients and are calculated as following.

$$a_0 = \frac{1}{\pi} \int_0^{2\pi} v(\omega t) d(\omega t) \tag{2}$$

then:

$$a_n = \frac{2V_o}{n\pi} \sin\left[n\varphi_1 \left(1 - \cos(n\pi)\right)\right] \tag{3}$$

Therefore, if n is even, then $a_n = 0$ and if n is odd, then $a_n = \frac{4V_0}{n\pi} \sin n\varphi_1$.

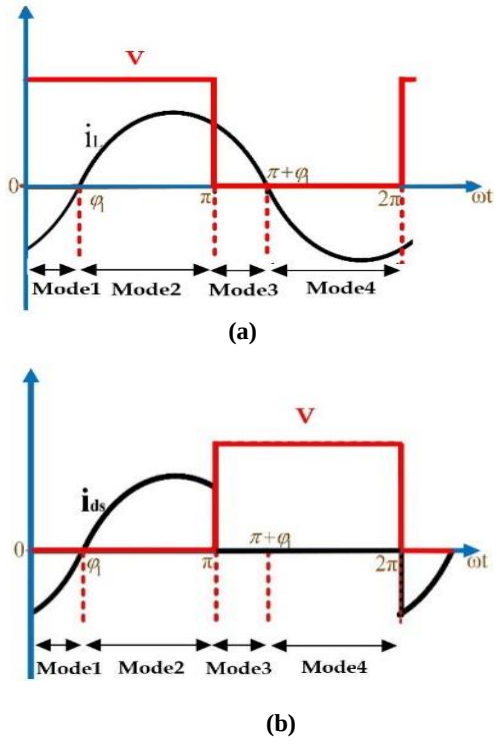

Fig. 5. (a) Current of resonant inductor. (b) Voltage and current of switch S_1 during different operation modes.

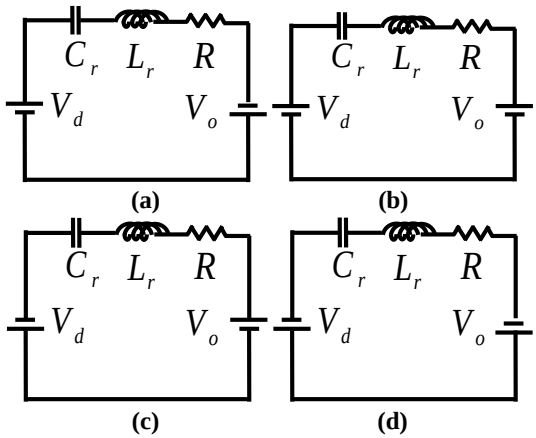

Fig. 6. Equivalent circuit in different operational modes: (a)mode 1 (b) mode 2 (c) mode 3 (d) mode 4.

Moreover, b_n is calculated similar to a_n as following:

$$b_n = \frac{1}{n\pi} \left[1 - \cos(n\pi)\right] \left[V_d - 2V_o \cos(n\varphi_1)\right] \tag{4}$$

Accordingly, if n is even, then bn=0 and if n is odd, then $b_n = \frac{2}{n\pi} \left[V_d - V_0 \cos\left(n\varphi_1\right)\right]$.

Combining the above equations, Cn could be calculated as following:

$$C_n = \sqrt{{a_n}^2 + {b_n}^2} = \frac{2}{n\pi} \sqrt{4{V_o}^2 + {V_d}^2 - 4V_d V_o \cos(n\varphi_1)} \tag{5}$$

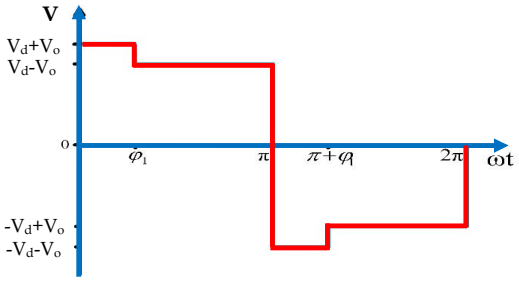

Fig. 7. Equivalent DC voltages in a period.

Therefore:

$$\phi_n = tan^{-1}(\frac{a_n}{b_n}) = tan^{-1}\left[\frac{2V_o \sin(n\varphi_1)}{V_d - 2V_o \cos(n\varphi_1)}\right] \quad (6)$$

The fundamental harmonic of $v(t)$ is as following:

$$v_1(t) = \frac{2}{\pi}\sqrt{4{V_o}^2 + {V_d}^2 - 4V_d V_0 \cos\varphi_1}. \sin\left[\omega t + \tan^{-1}\left(\frac{2V_o \sin\varphi_1}{V_d - 2V_o \cos\varphi_1}\right)\right] \quad (7)$$

The mentioned equivalent circuit steady state model could be simplified as one circuit indicated in Fig. 8.

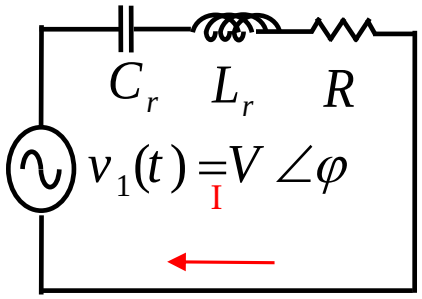

Fig. 8. Steady state model of the proposed driver.

where:

$$I = \frac{V\angle\varphi}{R + j(X_L - X_C)} \quad (8)$$

thus:

$$|I| = \frac{V}{\sqrt{R^2 + (X_L - X_C)^2}}\ ;\ \angle I = \varphi - \tan^{-1}\left(\frac{X_L - X_C}{R}\right) \quad (9)$$

then the output power could be achieved as:

$$P_{out(\max)} = R|I|^2 = \frac{RV^2}{R^2 + Z^2} \quad (10)$$

where,

$$|Z| = X_L - X_C$$

, The output power in j^{th} channel is obtained as:

$$P_{out(j)} = \frac{N_S}{N_{S\max}} P_{out(\max)};\quad N_{S\min} < N_S < N_{S\max} \quad (11)$$

where $N_{S\max} = {f_s}/{f_{\dim}}$ and $N_{S(j)} = {T_{on(j)}}/{T_{burst}}$ then:

$$P_{out(j)} = \frac{f_{\dim}^2}{f_s} \cdot T_{on(j)} P_{out(\max)};\quad 0 < T_{on(j)} < T_{burst} \quad (12)$$

3. POWER ANALYSIS

In this section, LED driver circuit is simplified as Fig. 9 and analysis with assuming high quality series resonant tank.

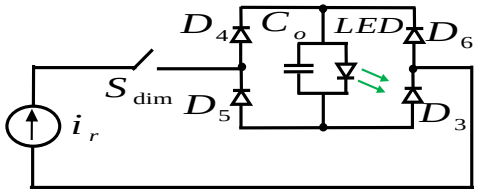

Fig. 9. Simplified circuit of the proposed driver.

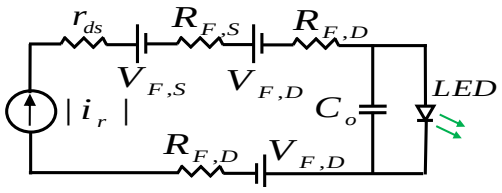

Fig. 10. Simplified equivalent circuit of the proposed driver.

Fig. 9 is simplified as Fig. 10 that r_{ds} is the total resistance between the drain and source of dim switch and $V_{F,S}$ is threshold voltage of the parallel inverse diode of the switch and $R_{F,S}$ is conductance resistance of reverse diode of dim switch and $V_{F,D}$ is forward voltage of diode and RF,D is conductance resistance of diode.
Output current is:

$$I_O = \frac{1}{2\pi}\int_0^{2\pi} i_r(t)d(\omega t) = \frac{I_{rm}}{\pi}\int_0^{\pi} \sin\omega t d(\omega t) = \frac{2I_{rm}}{\pi} \quad (13)$$

where I_{rm} is the maximum peak value of output current.
The input power is:

$$P_i = \frac{I_{rm}^2 R_i}{2} = \frac{\pi^2 I_o^2 R_i}{8} \quad (14)$$

Where R_i is the rectifier input resistance. The rms value of the current through each diode is:

$$I_{Drms} = \sqrt{\frac{1}{2\pi}\int_0^{2\pi} {i_{Di}}^2 d(\omega t)} = \sqrt{\frac{I_{rm}^2}{2\pi}\int_0^{\pi} \sin^2\omega t d(\omega t)} = \frac{I_{rm}}{2} = \frac{\pi I_o}{4} \quad (15)$$

The power loss in the diode forward resistance RF is calculated as:

$$P_{RF} = R_F I_{Drms}^2 = \frac{\pi^2 R_F}{16 R_L} P_o \quad (16)$$

Power loss in each diode due to diode forward voltage V_F is:

$$P_{VF} = V_F I_D = \frac{V_F I_o}{2} = \frac{V_F}{2V_o} P_o \quad (17)$$

Thus, the total conduction loss per diode is:

$$P_D = P_{VF} + P_{RF} = P_o\left(\frac{V_F}{2V_o} + \frac{\pi^2 R_F}{16 R_L}\right) \quad (18)$$

Current through the output capacitor can be approximated by:

$$i_{Co} \approx i_r - I_o = I_o \left(\frac{\pi}{2} |\sin(\omega t)| - 1 \right) \quad (19)$$

And its rms value is:

$$I_{Co(rms)} = \sqrt{\frac{1}{2\pi} \int_0^{2\pi} i_{Co}^2 d(\omega t)} = I_O \sqrt{\frac{\pi^2}{8} - 1} \quad (20)$$

Then the power loss in capacitor's ESR (r_{Co}) is calculated as:

$$P_{rCo} = r_{Co} I_{Co(rms)}^2 = r_{Co} I_o^2 (\frac{\pi^2}{8} - 1) = \frac{r_{Co}}{R_L} \left(\frac{\pi^2}{8} - 1 \right) P_o \quad (21)$$

The total conduction loss is as:

$$P_{cond} = 6P_D + 2P_{sw} + P_{rCo} = P_o [\frac{3V_F}{V_o} + \frac{3\pi^2 R_F}{8R_L} + \frac{\pi^2 r_{ds}}{8R_L} + \frac{r_{Co}}{R_L} (\frac{\pi^2}{8} - 1)] \quad (22)$$

The input power is expressed as:

$$P_i = P_o + P_{cond} = P_o [1 + \frac{3V_F}{V_o} + \frac{3\pi^2 R_F}{8R_L} + \frac{\pi^2 r_{ds}}{8R_L} + \frac{r_{Co}}{R_L} (\frac{\pi^2}{8} - 1)] \quad (23)$$

So the bridge rectifier efficiency is achieved as:

$$\eta_R = \frac{P_o}{P_i} = \frac{1}{1 + \frac{3V_F}{V_o} + \frac{3\pi^2 R_F}{8R_L} + \frac{\pi^2 r_{ds}}{8R_L} + \frac{r_{Co}}{R_L} (\frac{\pi^2}{8} - 1)} \quad (24)$$

The bridge rectifier efficiency could be achieved from the above equation. The used specifications are assumed as: $r_c = 0.05\Omega$, $R_o = 20\Omega$, $V_F = 1.25V$, $R_F = 0.21\Omega$ and $r_{ds} = 0.27\Omega$. Accordingly, the estimated efficiency of bridge rectifier is obtained 0.87.

4. DESIGN EXAMPLE

Temperature changes are ignored in the design of the converter elements. The input voltage is assumed to be 380V and the output voltage is 33V and switching frequency is chosen 65kHz. Reference [17] has reported that switching frequency must be more than 200Hz to prevent flicker. So in this paper, dimming frequency is chosen 500Hz to eliminate all of flickering effects. Dimming frequency was chosen low frequency to reduce switching losses and eliminate zero current control circuits. Following steps is follow to design the resonant components. Resonant frequency is presented as following:

$$f_r = \frac{1}{2\pi\sqrt{L_r C_r}} \quad (25)$$

Switching frequency is selected four time of resonant frequency to achieve ZVS condition [14]. Fig. 11 shows the block diagram of the proposed driver, where Ri is input resistor and MVR is voltage gain of bridge rectifier, MVS is half-bridge inverter's voltage gain and R is total resistance of converter. Then we have:

Switching frequency is selected four time of resonant frequency to achieve ZVS condition [14]. Fig. 11 shows the block diagram of the proposed driver, where Ri is input resistor and M_{VR} is voltage gain of bridge rectifier, M_{VS} is half-bridge inverter's voltage gain and R is total resistance of converter. Then we have:

$$R_i = \frac{8R_o}{\pi^2 \eta_R} = \frac{8 \times 20}{0.87\pi^2} \simeq 18.6\Omega \quad (26)$$

$$M_{VR} = \frac{\pi.\eta_R}{2\sqrt{2}} = \frac{0.87\pi}{2\sqrt{2}} \simeq 0.97 \quad (27)$$

$$M_{VS} = \frac{\sqrt{2}}{\pi} \simeq 0.45 \quad (28)$$

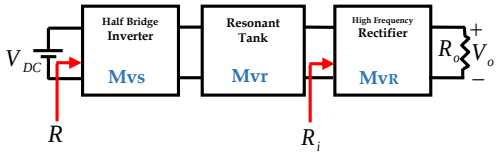

Fig. 11. Block diagram of proposed converter.

M_v and M_{vr} are assumed total voltage gain of half-bridge SRC and voltage gain of the SRC, respectively. Then we could be obtained as following:

$$M_V = \frac{V_o}{V_{DC}} = \frac{33}{380} = 0.086 \quad (29)$$

$$M_{Vr} = \frac{M_V}{M_{VS}.M_{VR}} = \frac{0.086}{0.45 \times 0.97} \simeq 0.2 \quad (30)$$

Quality factor (Q_L) is presented as equation (32) where η_1 is estimated efficiency of half-bridge SRC with bridge rectifier. Switching frequency and resonant frequency is shown with f_s and f_r respectively. With a η_1 of 0.99 and f_s of 65kHz, quality factor Q_L and R are calculated as following:

$$Q_L = \frac{\sqrt{\frac{{\eta_1}^2}{{M_{vr}}^2} - 1}}{\left| \frac{f_s}{f_r} - \frac{f_r}{f_s} \right|} = \frac{\sqrt{\frac{0.99^2}{0.2^2} - 1}}{\left| \frac{65}{16} - \frac{16}{65} \right|} \simeq \frac{4.61}{3.816} \simeq 1.27 \quad (31)$$

$$R = \frac{R_i}{\eta_1} = \frac{18.6}{0.99} \simeq 18.8 \quad (32)$$

Resonant inductance and resonant capacitor could be presented as:

$$L_r = \frac{Q_L.R}{\omega_r} = \frac{1.27 \times 18.8}{2\pi \times 16} \simeq 237\mu H \quad (33)$$

$$C_r = \frac{1}{L_r.{\omega_r}^2} = \frac{1}{237 \times (2\pi \times 16)^2} = 417nF \quad (34)$$

5. SIMULATION RESULTS

In this study, the proposed converter is drawn in PSCAD software and is placed the values of the elements from the catalogue in the software to make the results closer to reality. A two-channel adjustable converter with 10-W LED strings is simulated and the simulation results of the proposed converter are presented, which confirms the theoretical issues.

Fig. 12 is shown the simulated LED driver with two 10-W LED. The characteristics of the proposed driver and the simulated values of the resonance inductor and capacitor close to the computational values were selected according to Table 1. D-flip flop, comparator, signal generator and mono-stable multi vibrator are used to control the switches and brightness of each channel is controlled by duty cycle of dim switches. Fig. 13 shows ZVS operating of two main switches and Fig. 14 shows output voltage and current of two channels that the brightness of

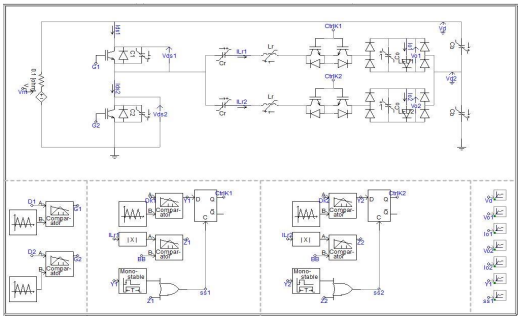

Fig. 12. simulated converter of two channel dimmable LED driver.

channel1 and channel2 were adjusted to duty cycles 0.3 and 0.7, respectively. As can be seen, the output voltage of channel 1 is 32V and its current is 160mA and the output voltage of channel 2 is 36V and its current is 370mA. Waveforms of the resonant circuit currents were measured, as shown in Fig. 15(a) and 15(b)

Table 1. Circuit components and parameters

Description	Symbol	Value
Input DC voltage	$2V_d$	380V
DC-link capacitors	C_1 and C_2	$220\mu F$
Resonance inductor	L_r	$240\mu H$
Resonance capacitance	C_r	390 nF
Switches	S_i	IRFP460
Switching frequency	f_s	65kHz
Output Capacitor	C_o	$1000\mu F$
Rectifier Diodes	D_3, D_4, D_5, D_6	BY399
LED Lamp	LED	$2 \times 10W$

In Figs. 16-18 experimental results is shown. Fig. 16 shows voltage and current of switch S1 and verifies ZVS operation of switching like simulation result. Fig. 18(a) is regulated on 30% duty cycle and Fig. 18(b) is regulated on 70% duty cycle. It is shown output voltage in Fig. 18 (top) and output current in Fig. 17 (bottom) that verify output DC voltage (top) and current (bottom). All of these experimental results verify simulation results.

Moreover, the efficiency of the proposed driver versus output power at different burst duty cycles is shown in Fig. 19. As indicated, the driver efficiency is improved and maximum efficiency of 90% is achieved at 10W output power and unity burst duty cycle.

A comparison study of the proposed driver with other recent topologies is done in the Table 2. As indicated, the proposed driver is capable of single-stage power conversion, independent dimming, and soft-switching even with reasonable number of employed components.

According to Figs. 20 and 21, the number of switches per channel and the number of windings versus the number of channels in the proposed converter is better than the other references. Only [10] has a smaller number of switches, which in turn has a much larger number of coils. Table 2 summarizes the comparison of the proposed converter with recent converters. In this comparison, the number of circuit stages, the number of switches, the number of inductors and transformers, the

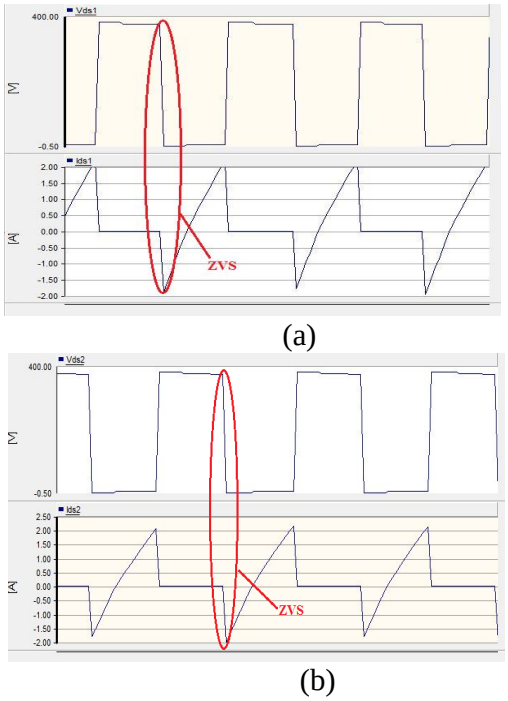

Fig. 13. The simulated waveforms of switches voltage and current and its ZVS operation. (a) S_1 waveforms (b) S_2 waveforms.

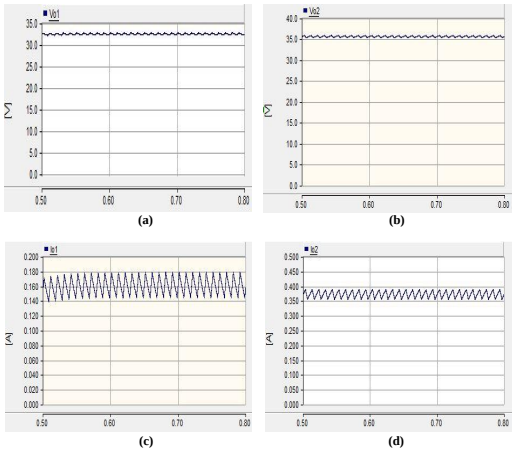

Fig. 14. The simulated waveforms of output voltage and output current (a),(c) V_{out} and I_{out} of channel 1 with duty cycle 30%, respectively (b),(d) V_{out} and I_{out} of channel 2 with duty cycle 70%, respectively.

dimming status, the switching status, maximum efficiency and the dimming strategy are given. Generally, the other structure that is provided in Table 2 has some advantages and some disadvantages compared to the proposed structure. Switches in power electronics converters have high losses and each one requires control circuit. Decreasing the number of switches can reduce losses and improve converter efficiency and reliability. The number of switches used in the proposed converter is less than recent papers [14, 15] and more than [10–12, 16]. The four references [10–12, 16] have fewer switches than our proposed converter, but [10, 16] are multi-stage and less efficiency. In

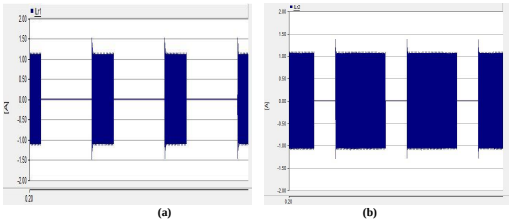

Fig. 15. The current of i_L in two channel driver with burst duty cycle of (a) 30% and (b) 70%.

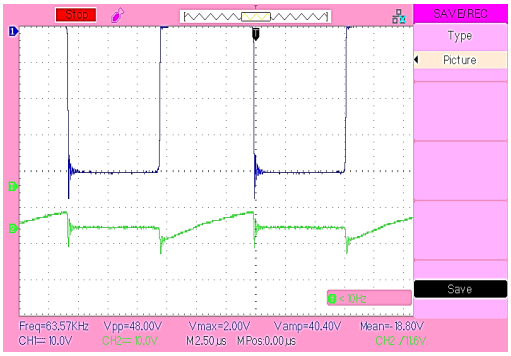

Fig. 16. The experimental waveforms of switche voltage (top) and current (bottom) and its ZVS operation.

Fig. 17. Output voltage (top) and current (bottom).

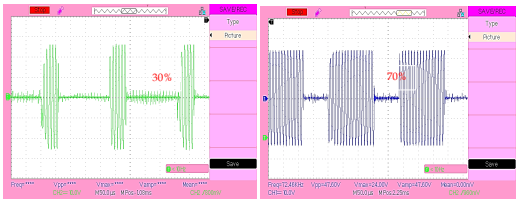

Fig. 18. The current of i_L in duty cycle of 30% (left) and 70% (right).

addition, switching in [10] is hard and it has huge configuration because of variable inductor. [12] has more efficiency than our proposed converter but it has not independent dimming capability and [11] has equal efficiency with proposed converter but it has large volume because of variable inductor.

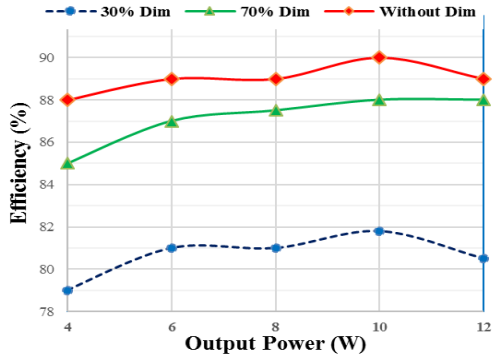

Fig. 19. Efficiency of converter in 30, 70 and 100 percentage duty.

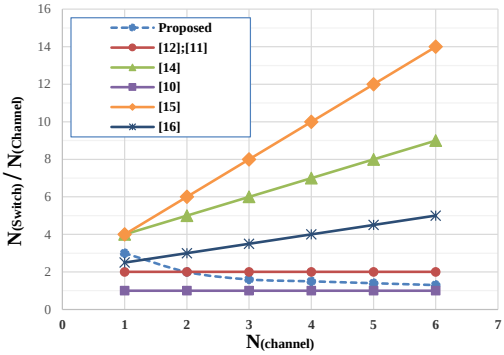

Fig. 20. ($N_{SWITCH}/N_{CHANNEL}$) versus $N_{CHANNEL}$.

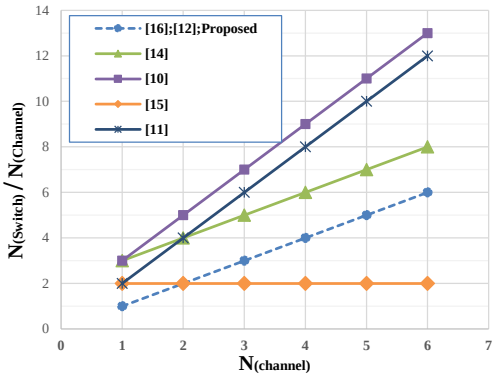

Fig. 21. (N_{Trans} & Inductor $/N_{CHANNEL}$) versus NCHANNEL.

6. CONCLUSION

The proposed circuit provides a multi-channel LED driver structure with independent dimming for lighting applications in DC grids. The proposed driver consists of two switches with half-bridge structure, two capacitors of voltage divider, SRC, full-bridge rectifier and dimming switch. A 20-watt two-channel LED driver was simulated with an input voltage of 380 volts, which confirmed the theoretical analyses. Independent dimming capability and operation with constant switching frequency and soft switching operation and the ability to easily expand to multi-channel are the most important advantages of this driver.

Table 2. Comparison of the existing for n-channel dc/dc stage of led drivers

Reference	No. of Stage	Switch Number	No.of Transformer and Indicators	Independent Dimming	Switching State	Dimming Strategy	DC bus Voltage (V)	Output Power (W)	Maximum Efficiency (%)
[10]	2	1	2N+1	Yes	Hard Switching	Variable Inductor	48V	54.4	88
[11]	1	2	2N	Yes	Soft Switching	Variable Inductor	380V	50	90
[12]	1	2	N	No	Soft Switching	Switching Frequency	100V	58	93.5
[14]	1	N+3	N+2	No	Partial Soft Switching	PWM	400V	100	94
[15]	2	2N+2	2	Yes	Partial Soft Switching	AM/BL-PWM	400V	60	85.5
[16]	3	N/2+2	N	Yes	Soft Switching	AM	48V	20	90
Proposed	1	N+2	N	Yes	Soft Switching	Burst Control	380V	20	90

REFERENCES

1. CAO, L., ZHU, Y., WU, H., “A New Electrolytic Capacitor-less LED Driver with Coupled-Inductor,” In: 2020 IEEE Applied Power Electronics Conference and Exposition (APEC). IEEE, pp. 1537-1543, 2020.
2. S. Porpandiselvi, N.Vishwanathan, and APPLICATIONS, "A three-leg resonant converter for two output LED lighting application with independent control," IET Power Electronics, vol. 47, no. 7, pp. 1173-1187, 2019.
3. Liu, T., Liu, X., He, M., Zhou, S., Meng, X. and Zhou, Q., Flicker-Free Resonant LED Driver With High Power Factor and Passive Current Balancing. IEEE Access, vol. 9, pp. 6008-6017, 2020.
4. C. A. Cheng, T. Chung, "A single-stage LED streetlight driver with PFC and digital PWM dimming capability," Int J Circuit Theory Appl, vol. 44, no. 11, pp. 1942-1958, 2016.
5. J. M. Wang, S. T. Wu, S. C. Yen, J. Lin, "A simple control scheme for a single stage flyback LED driver," Int J Circuit Theory Appl, vol. 43, no. 12, pp. 1879-1898, 2015.
6. C. Ye, P. Das, and S. K. J. I. T. o. I. E. Sahoo, "Peak Current Control of Multi-Channel LED Driver with Selective Dimming," IEEE Transactions on Industrial Electronics, 2018.
7. Torkaman, H., Karami, N., & Nezamabadi, M. "Design, simulation, validation and comparison of new high step-up soft switched converter for fuel cell energy system." Journal of Energy Management and Technology, 1(1), 53-60, 2017.
8. Maalandish, M., Pourjafar, S., Hosseini, S. H., & Taghizadegan Kalantari, N. "Leakage current elimination with improved non-isolated nine-level inverter for grid-connected PV panels." Journal of Energy Management and Technology, 1(2), 46-55, 2017.
9. Sedaghati, F., Mohammad Salehian, S., Shayeghi, H., & Shokati Asl, E. "A configuration of double input Z-source DC-DC converter for standalone PV/battery system application." Journal of energy management and technology, 2(3), 60-69, 2018.
10. R. A. Pinto, J. M. Alonso, M. S. Perdigão, M. F. da Silva, and R. N. do Prado, "A new technique to equalize branch currents in multiarray LED lamps based on variable inductors," IEEE Transactions on Industry Applications, vol. 52, no. 1, pp. 521-530, 2016.
11. J. M. Alonso, M. S. Perdigão, M. A. Dalla Costa, G. Martínez, and R. Osorio, "Analysis and Experiments on a Single-Inductor Half-Bridge LED Driver With Magnetic Control," IEEE Transactions on Power Electronics, vol. 32, no. 12, pp. 9179-9190, 2017.
12. T. N. Gücin, B. Fincan, and M. J. I. T. o. P. E. Biberoğlu, "A Series Resonant Converter-Based Multichannel LED Driver With Inherent Current Balancing and Dimming Capability," IEEE Transactions on Power Electronics, vol. 34, no. 3, pp. 2693-2703, 2018.
13. W. Feng, F. C. Lee, and P. Mattavelli, "Optimal trajectory control of burst mode for LLC resonant converter," IEEE Transactions on Power Electronics, vol. 28, no. 1, pp. 457-466, 2013.
14. H. Ma, J.-S. J. Lai, C. Zheng, and P. Sun, "A high-efficiency quasi-single-stage bridgeless electrolytic capacitor-free high-power AC–DC driver for supplying multiple LED strings in parallel," IEEE Transactions on Power Electronics, vol. 31, no. 8, pp. 5825-5836, 2016.
15. C. Wong, K. Loo, H. H.-C. lu, Y. Lai, M. H. Chow, and K. T. Chi, "Independent Control of Multicolor-Multistring LED Lighting Systems With Fully Switched-Capacitor-Controlled $ LCC $ Resonant Network," IEEE Transactions on Power Electronics, vol. 33, no. 5, pp. 4293-4305, 2018.
16. J. Liu, W. Sun, and J. J. I. P. E. Zeng, "Precise current sharing control for multi-channel LED driver based on switch-controlled capacitor," IET Power Electronics, vol. 10, no. 3, pp. 357-367, 2017.
17. Y. Ko, H.-S. Cho, S.-S. Lee, S.-B. Shin, Y. Song, and S.-G. Lee, "A compact flicker-free transformer-less LED driver with an enhanced power factor for omnidirectional multichannel smart bulb applications," IEEE Transactions on Power Electronics, vol. 31, no. 8, pp. 5851-5862, 2015.